CHEMISTRY OF MATERIALS
Article

Chem. Mater. **2010,** *22,* 6509–6517 6509
DOI:10.1021/cm103148n

Sol−Gel Based Chemical Synthesis of $Nd_2Fe_{14}B$ Hard Magnetic Nanoparticles

Pratap K. Deheri,*,† Viswanathan Swaminathan,*,† Shekhar D. Bhame,*,† Zhongwu Liu,*,‡ and Raju V. Ramanujan*,†

†*School of Materials Science and Engineering, Nanyang Technological University, Singapore 639798, Singapore, and* ‡*School of Materials Science and Engineering, South China University of Technology, Guangzhou 510640, PR China*

Received November 2, 2010

$Nd_2Fe_{14}B$ hard magnetic nanoparticles were synthesized by chemical synthesis techniques. Nd−Fe−B gel was prepared using $NdCl_3 \cdot 6H_2O$, $FeCl_3 \cdot 6H_2O$, H_3BO_3, citric acid, and ethylene glycol (EG) by a Pechini type sol−gel method. This gel was subsequently annealed to produce mixed oxide powders. $Nd_2Fe_{14}B$ nanoparticles were prepared from these oxides by a reduction−diffusion process. The phase analysis, structure, and magnetic properties were determined by Fourier transform infrared spectroscopy (FTIR), nuclear magnetic resonance (NMR), X-ray diffraction (XRD), field emission scanning electron microscope (FESEM), transmission electron microscope (TEM), and vibrating sample magnetometer (VSM) techniques. The mechanism of $Nd_2Fe_{14}B$ formation was investigated by differential scanning calorimetry (DSC), XRD, and thermodynamic free energy change data. Our experimental and modeling results showed that the reduction−diffusion of the Nd−Fe−B mixed oxide was a three step process. The reduction of Fe_2O_3 to Fe and B_2O_3 to B occurred at 300 °C. NdH_2 and Fe was formed from Nd_2O_3 and $NdFeO_3$ at 620 °C. The $Nd_2Fe_{14}B$ phase was formed from NdH_2, Fe, and B at 692 °C. The coercivity of as-synthesized powder was 6.1 kOe. The Henkel plot showed that this powder was exchange coupled; removal of CaO by washing led to dipolar interactions and a decrease in coercivity.

1. Introduction

Research in the area of magnetism and magnetic materials is a rich combination of synthesis, characterization, theoretical concepts, and engineering applications.[1] Hard magnetic materials are used in hard disk drives, motors, generators, loudspeakers, magnetic sensors, etc. Polymer−magnetic powder composites are used in several applications including electromagnetic actuation micropumps.[2] Since the discovery of the excellent magnetic properties of $Nd_2Fe_{14}B$ hard magnetic alloys,[3] intense research has been focused on novel synthesis techniques and optimum microstructural development. The most commonly used process for producing $Nd_2Fe_{14}B$ magnetic alloys are powder metallurgy methods[3] and rapid quenching techniques.[4,5] These methods are energy intensive and require high purity elements as starting materials. To prepare $Nd_2Fe_{14}B$ based bonded magnets, sintered magnets, or magnetic elastomers for engineering applications, magnetic powders are essential.[6,7] Typically, magnetic flakes from melt spinning or ingots are crushed, ball milled, or subjected to hydrogenation, dispropornation desorption, and recombination treated (HDDR) to obtain micrometer sized powders.[6,7] Magnetic nanoparticles are needed in ferrofluids,[8] refrigeration systems,[9] and multiterabit information storage devices.[10,11] External manipulation of such magnetic nanoparticles facilitates their use in biomedical applications such as drug delivery, cancer therapy by hyperthermia, protein purification, and medical imaging.[11−15] Moreover, magnetic nanoparticles with a desired shape and size distribution are also of fundamental interest;[16] in the nanometer size range,

*To whom correspondence should be addressed. Tel: (65) 6790 4342. Fax: (65) 6790 9081. E-mail: Ramanujan@ntu.edu.sg.

(1) Coey., J. M. D. *J. Magn. Magn. Mater.* **2001**, *226−230*, 2107–2112.
(2) Yamahata, C.; Lotto, C.; Al-Assaf, E.; Gijs, M. A. M. *Microfluid. Nanofluid.* **2004**, *1*, 197–207.
(3) Sagawa, M.; Fujimura, S.; Togawa, N.; Yamamoto, H.; Matsuura, Y. *J. Appl. Phys.* **1984**, *55*, 2083–2087.
(4) Croat, J. J.; Herbst, J. F.; Lee, R. W.; Pinkerton, E. F. *J. Appl. Phys.* **1984**, *55*, 2078–2082.
(5) Koon, N. C.; Das, B. N. *J. Appl. Phys.* **1984**, *55*, 2063–2066.
(6) Brown, D.; Ma, B.-M.; Chen, Z. *J. Magn. Magn. Mater.* **2002**, *248*, 432–440.
(7) Setnescu, R.; Setnescu, T.; Jipa, S.; Kappel, W.; Dumitru, M.; Codescu, M. M.; Stancu, N.; Zaharescu, T. *J. Optoelectron. Adv. Mater.* **2006**, *8*, 533–536.
(8) Sahoo, Y.; Goodarzi, A.; Swihart, M. T.; Ohulchanskyy, T. Y.; Kaur, N.; Furlani, E. P.; Prasad, P. N. *J. Phys. Chem. B* **2005**, *109*, 3879–3885.
(9) Shull, R. D. *IEEE Trans. Magn.* **1993**, *29*, 2614–2615.
(10) Sun, X.; Huang, Y.; Nikles, D. E. *Int. J. Nanotechnol.* **2004**, *1*, 328–346.
(11) Hyeon, T. *Chem. Commun.* **2003**, *8*, 927–934.
(12) Gao, J.; Gu, H.; Xu, B. *Acc. Chem. Res.* **2009**, *42*, 1097–1107.
(13) Alexiou, C.; Schmid, R. J.; Jurgons, R.; Kremer, M.; Wanner, G.; Bergemann, C.; Huenges, E; Nawroth, T.; Arnold, W.; Parak, F. G. *Eur. Biophys. J.* **2006**, *35*, 446–450.
(14) Ang, K. L.; Venkatraman, S.; Ramanujan, R. V. *Mater. Sci. Eng., C* **2007**, *27*, 347–351.
(15) Sellmyer, D.; Skomski, R. *Advanced magnetic nanostructures*; Springer: New York, 2006.
(16) Petit, C.; Taleb, A.; Pileni, M. P. *J. Phys. Chem. B* **1999**, *103*, 1805–1810.

© 2010 American Chemical Society
Published on Web 11/30/2010

magnetic nanoparticles are used to explore anisotropy, exchange coupling, and the magnetism of single domain particles.[15] The size and temperature dependence of the magnetic properties of nanoparticles has stimulated research to overcome the conventional limits of magnetic data storage.[15]

Chemical synthesis methods have been widely used to prepare nanostructured materials.[11] In recent years, synthesis of $Nd_2Fe_{14}B$ magnets by chemical routes has been attempted; one such method involves reduction of suitable salts of iron and neodymium by sodium borohydride.[17,18] Another is the polyol reduction method;[19] the organometallic complex of iron and neodymium is reduced by a polyalcohol. However, due to a high negative reduction potential of the rare earth element (−2.43 eV), it is quite difficult to coreduce rare earth and transition metals simultaneously (−0.057 eV).[20,21] $Nd_2Fe_{14}B$ alloys are reactive and oxidation prone, making synthesis of nanoparticles challenging.[21] In chemical methods, nanoparticle size can be controlled by adjusting reaction parameters such as time, temperature, and concentration of reagents.[11,22,23] Particle growth can be minimized by controlling the reaction temperature and time.[23] Alloying to improve magnetic properties can also be more readily accomplished by chemical synthesis techniques. In this work, the sol−gel technique was used to synthesize a chemically homogeneous oxide; reduction−diffusion of this oxide produced $Nd_2Fe_{14}B$ magnetic nanoparticles.

$Nd_2Fe_{14}B$ synthesis by reduction−diffusion techniques and their magnetic properties have been reported.[24−29] In previous work, a combustion method followed by reduction−diffusion was used to synthesize exchange coupled $Nd_2Fe_{14}B$−α-Fe nanocomposites in the 5−20 nm size range.[29] However, the mechanism of this process is still not well understood. Hence, we report the synthesis and formation mechanism of $Nd_2Fe_{14}B$ nanoparticles produced by sol−gel followed by reduction−diffusion. Such solution based synthesis combined with high temperature solid state reduction has been proved to be a successful method in the synthesis of hard nanocrystalline magnetic materials.[30] Our results show that reduction−diffusion can be carried out at lower temperatures and times than those reported earlier.[24−27] As a result, fine $Nd_2Fe_{14}B$ nanoparticles of ∼65 nm size were successfully synthesized by this method. This technique can be readily extended to the synthesis of exchange-coupled magnetic nanoparticles to obtain high energy product magnets. Magnetic measurements showed that the coercivity of the as-synthesized powder was 6.1 kOe. Ferromagnetic interparticle interactions were studied using the Henkel plot; the as-synthesized powder was exchange coupled, and removal of CaO by washing resulted in dipolar interactions.

2. Experimental Section

2.1. Characterization Techniques. X-ray diffraction (XRD) was measured using a Bruker AXS X-ray diffractometer (Cu Kα radiation, λ = 0.154 nm). For qualitative phase analysis, the XRD 2θ scan data were recorded in the range of 20−80°. For quantitative Rietveld analysis, the XRD data were recorded in the range of 20−120° with a step size 2θ of 0.01°. Rietveld refinement was carried out using the software program TOPAS 3. Tetragonal $Nd_2Fe_{14}B$ (space group $P4_2/mnm$), $Nd_2Fe_{14}BH_{4.7}$ (space group $P4_2/mnm$), and α-Fe (space group $Im\bar{3}m$) were taken as the starting model. Refinement was carried out in the following sequence: background, zero point shift, scale factor, unit cell constant, and crystal size. The infrred (IR) spectra were recorded on KBr pellet using a Perkin-Elmer Fourier transform infrared spectroscopy (FTIR) spectrometer. The ^1H NMR spectra was recorded at room temperature in D_2O solvent using a Bruker nuclear magnetic resonance (NMR) spectrometer at 300 MHz. The microstructure of the powders was examined by a JEOL JSM-6340F field emission scanning electron microscope (FESEM) and transmission electron microscope (JEOL TEM 2010, 200 kV). Room temperature magnetic measurements were performed at a magnetic field strength up to 1.5 T using a Lakeshore 7400 vibrating sample magnetometer (VSM).

2.2. Nd−Fe−B Oxide Synthesis by Sol−Gel Process. Neodymium chloride hexahydrate ($NdCl_3 \cdot 6H_2O$, 99.9%), iron chloride hexahydrate ($FeCl_3 \cdot 6H_2O$, 97−102%), boric acid (H_3BO_3, 99.8%), citric acid (99.5%), and ethylene glycol (99%) from Alfa Aesar were used for the synthesis. The synthesis of Nd−Fe−B oxide powder was carried out by a Pechini type sol−gel process.[31] In a typical experiment, for a nominal composition of $Nd_{15}Fe_{77.5}B_{7.5}$, stoichiometric amounts of neodymium chloride hexahydrate, iron chloride hexahydrate, and boric acid were dissolved in deionized water. Then, citric acid and ethylene glycol in a 2:1 molar ratio to metal salts were added to prepare a thermally stable sol. Finally, the mixed solution was heated at 90 °C overnight resulting in a viscous gel. This gel was characterized by FTIR and NMR spectrometry. The gel was then dried at 200 °C. The dried gel was then heated at 400 °C for 2 h, followed by 800 °C for 2 h to prepare Nd−Fe−B oxide powder. These powders were analyzed by X-ray diffraction, FTIR spectrometry, TEM, and VSM. This powder was subjected to the reduction−diffusion process to obtain the desired $Nd_2Fe_{14}B$ phase.

2.3. $Nd_2Fe_{14}B$ Synthesis. $Nd_2Fe_{14}B$ powder was synthesized by mixing Nd−Fe−B oxides powder with 1.5 wt % of CaH_2 and annealing at 800 °C for 2 h in vacuum. CaH_2 (90−95%, Sigma Aldrich) was used as the reducing agent instead of calcium metal due to the ease of mixing. Moreover, pulverization caused by

(17) Haik, Y.; Chatterjee, J.; Chen, C. J. *J Nanopart. Res.* **2005**, *7*, 675–679.
(18) Km, C. W.; Km, Y. H.; Cha, H. G.; Kang, Y. S. *Phys. Scr.* **2007**, *T129*, 321–325.
(19) Cha, H. G.; Kim, Y. H.; Kim, C. W.; Kang, Y. S. *IEEE Trans. Magn. NMDC* **2006**, *1*, 656–657.
(20) Lee, J. D. *Concise Inorganic Chemistry*; Blackwell Science: Oxford, UK, 1998; pp 173 and 861.
(21) Chinnasamy, C. N.; Huang, J. Y.; Lewis, L. H.; Latha, B.; Vittoria, C.; Harris, V. G. *Appl. Phys. Lett.* **2008**, *93*, 032505-1–032505-3.
(22) Gu Kwon, S.; Hyeon, T. *Acc. Chem. Res.* **2008**, *41*, 1696–1709.
(23) Murray, C. B.; Sun, S.; Gaschler, W.; Doyle, H.; Betley, T. A.; Kagan, C. R. *IBM J. Res. Dev.* **2001**, *45*, 47–56.
(24) Okajima, Y.; Tsugita, Y.; Takechi, T.; Okada, S. U.S. Patent 4,681,623, 1987.
(25) Ohmori, K.; Shionoya, K. *J. Appl. Phys.* **1991**, *69*, 5504–5506.
(26) Sidhu, R. K. *J. Alloys Comp.* **2002**, *346*, 250–254.
(27) Jang, T. S.; Lee, D. H.; Yu, J. H.; Choi, C. J.; Seo, W. S.; Lee, H. Y. *Rare Met.* **2006**, *25*, 223–226.
(28) Dong, X. L.; Kim, B. K.; Choi, C. J.; Park, K. S.; Zhang, Z. D. *J. Mater. Res.* **2001**, *16*, 1083–1089.
(29) Bhame, S. D.; Swaminathan, V.; Deheri, P. K.; Ramanujan, R. V. *Adv. Sci. Lett.* **2010**, *3*, 1–6.
(30) Hou, Y.; Xu, Z.; Peng, S.; Rong, C.; Liu, J. P.; Sun, S. *Adv. Mater.* **2007**, *19*, 3349–3352.
(31) Pechini, M. P. U.S. Patent 3,330,697, 1967.

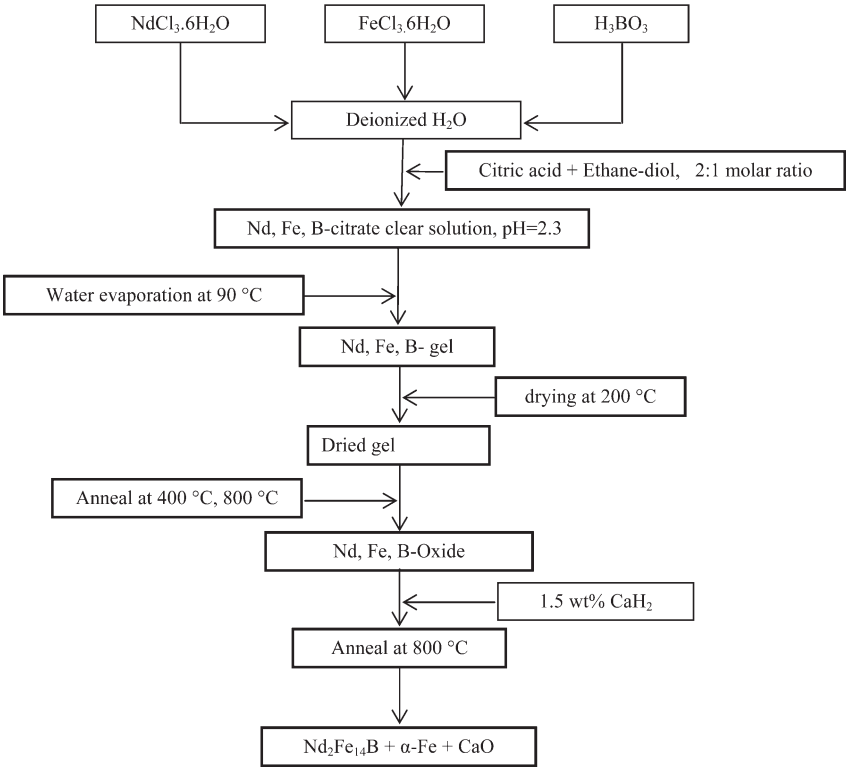

Figure 1. Flowchart of preparation of $Nd_2Fe_{14}B$ magnetic powder by sol−gel followed by reduction−diffusion process.

hydrogen gas released during heating, resulted in greater surface area and accelerate reduction. In this process, the major by-product was calcium oxide with residual calcium metal. To remove CaO, the reaction mixture was washed with dilute acetic acid and deionized water. Finally, the powder was washed with acetone followed by *n*-hexane and dried by vacuum evaporation. A schematic diagram of the synthesis process is shown in Figure 1. (*Hazard*: The CaH_2 and Ca can react vigorously with moisture/water and must be handled in a glovebox with appropriate personal protective equipment. The synthesized Nd−Fe−B nanoparticles were unstable to oxidation and must be handled in a glovebox.)

2.4. Study of Reaction Mechanism. To determine the mechanism of reduction of the oxide to form the $Nd_2Fe_{14}B$ phase, isochronal differential scanning calorimetry (DSC) measurements were carried out in argon at a heating rate of 20 K min^{-1} using a Netzch DSC-404. Nd−Fe−B oxides with 1.5 wt % of CaH_2 were heated for 2 h in vacuum at temperatures corresponding to the peak temperature obtained from the isochronal DSC study. At intermediate temperatures, the products of the reaction between Nd−Fe−B oxides and CaH_2 were unstable in the air; hence, for X-ray diffraction data collection, the reaction products were wrapped in parafilm inside a nitrogen glovebox.

3. Results and Discussion

3.1. $Nd_2Fe_{14}B$ Phase Formation from Nd−Fe−B Gel. *3.1.1. Nd−Fe−B Gel Formation.* The synthesis of $Nd_2Fe_{14}B$ is a two step process. The first step was the preparation of Nd−Fe−B-oxide by a modified Pechini type sol−gel method.[31] The second step was the reduction−diffusion of the oxide by CaH_2. The IR spectra and NMR results of the Nd−Fe−B gel are shown in Figure 2A,B. The broad absorption spectra at ∼3400 cm^{-1} was due to O−H stretching of free hydroxyl group from citric acid and metal citrate complex and the intermolecular hydrogen bonds.[32] The absorbance at ∼1731 (γ C═O) and ∼1202 cm^{-1} (γ C−O) were assigned to the carboxylate group, arising from the esterification reaction of both free and complex citric acid and ethylene glycol (EG).[32,33] The presence of metal coordinated citrate complex was consistent with the absorbance at 1622.4 cm^{-1} (γ_{as} COO) and 1393 cm^{-1} ((γ_s COO).[32,33] The difference ($\Delta\gamma = \gamma_{as} - \gamma_s$) suggested that −COO was coordinated to metal ion as a monodentate ligand.[34] ^{1}H NMR of the gel (Figure 2B) showed two broad peaks at 2.8 and 3.03 ppm from the citric acid methylene proton after esterification with ethylene glycol.[33] The proton of excess ethylene glycol appeared at 3.5 ppm.[32,33] There were five more peaks at 3.7 ppm and between 4.1 and 4.4 ppm, corresponding to the methylene proton in position α to the oxygen of ester or ether group following the esterification and esterification−etherization reaction.[32,33] Thus, the resulting gel was a metal citrate complex connected by EG via esterification reaction.

3.1.2. Annealing of Nd−Fe−B Gel. The Nd−Fe−B gel was heated in air to obtain Nd−Fe−B oxide. To study the phase evolution during annealing of this gel, it was heat treated for 2 h from 200 to 800 °C at temperature intervals of 100 °C. X-ray diffraction was performed after heat treatment to identify the phases (Figure 3). The as prepared gel and gel heated at 200 °C was amorphous. At 300 °C, an intermediate

(32) Montemayor, S. M.; Garcia-Cerda, L. A.; Torres-Lubian, J. R.; Rodriguez-Fernandez, O. S. *J. Sol-Gel Sci. Technol.* **2007**, *42*, 181–186.
(33) Montemayor, S. M.; Garcia-Cerda, L. A.; Torres-Lubian, J. R.; Rodriguez-Fernandez, O. S. *Mater. Res. Bull.* **2008**, *43*, 1112–1118.
(34) Kakihana, M.; Nagumo, T.; Okamoto, M.; Kakihana, H. *J. Phys. Chem.* **1987**, *91*, 6128–6136.

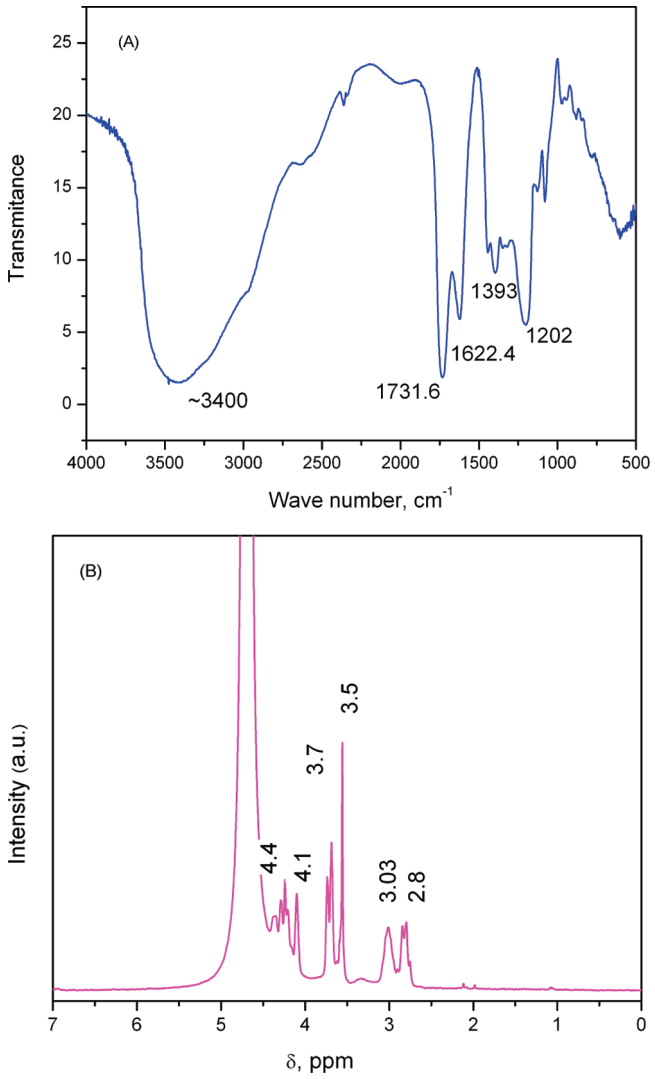

Figure 2. (A) IR spectra of Nd−Fe−B gel. The absorption at 1622.4 cm^{-1} (γ_{as} COO) and 1202 cm^{-1} (γ_s COO) are from metal coordinated citric acid and ethylene glycol ester. (B) ^1H NMR of Nd−Fe−B gel. The highest intensity peak at $\delta = 4.7$ is from DOH and is due to the proton exchange between solvent D_2O and citric acid.

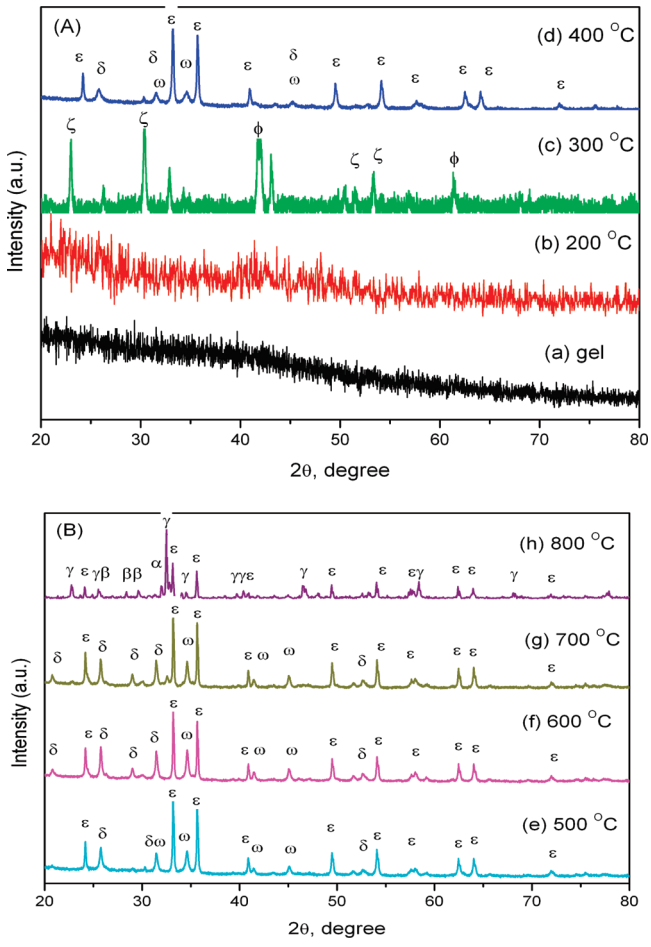

Figure 3. (A, B) (a) XRD patterns of NdFeB gel; (b−h) NdFeB gel annealed for 2 h, (b) 200 °C, (c) 300 °C, (d) 400 °C, (e) 500 °C, (f) 600 °C, (g) 700 °C, and (h) 800 °C. There are some unidentified peaks for gel annealed at 300 °C; ξ, $Nd_2O_2CO_3$; ϕ, FeO; ω, Fe_3BO_5; δ, $NdBO_3$; ε, Fe_2O_3; β, Nd_2O_3; α, B_2O_3; γ, $NdFeO_3$.

$Nd_2O_2CO_3$ phase was observed. At 400 °C, intermediate phases Fe_3BO_5 and $NdBO_3$ were formed; these two phases were stable up to 700 °C. Annealing at 800 °C resulted in the formation of Nd_2O_3, $NdFeO_3$, Fe_2O_3, and B_2O_3 phases. At 800 °C, Fe_3BO_5 reacted with $NdBO_3$ in the presence of oxygen to form $NdFeO_3$ and B_2O_3.

The IR spectrum of heat treated gel is shown in Figure 4. The intensities of broad absorption spectra at ~3400 cm^{-1}, the absorbance at 1622, 1731, 1393, and 1202 cm^{-1}, corresponding to the citrate complex, decreased with increasing temperature. For annealing temperatures of 500 °C, these peaks were not observed, indicating that annealing at 500 °C was sufficient to remove volatile organic materials. At temperatures between 600 and 800 °C, absorption bands at 760.2 cm^{-1} (B−O−B bending, boron oxygen network) and 730.6 cm^{-1} (B−O−B bending, bridge between BO_3 and BO_4^-) were

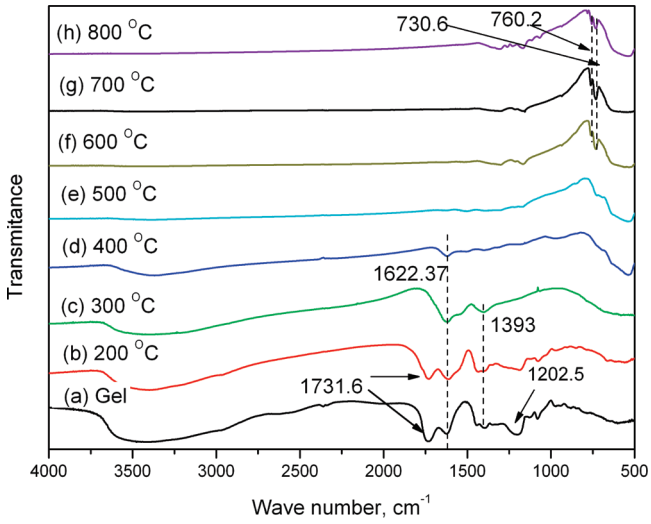

Figure 4. IR spectra of (a) Nd−Fe−B gel; (b−h) gel annealed in the temperature range of 200−800 °C for 2 h. Annealing at 500 °C removes all organic volatile materials.

observed, corresponding to the characteristic absorption of B_2O_3.[35,36] These results suggested that Fe_3BO_5 and $NdBO_3$ reacted at 600 °C to form $NdFeO_3$ and B_2O_3 phases. XRD observations showed B_2O_3 phase formation only at 800 °C,

(35) Toderas, M.; Filip, S.; Ardelean, I. *J. Optoelectron. Adv. Mater.* **2006**, *8*, 1121–1123.
(36) Kamitsos, E. I.; Karakassides, M. A.; Chryssikos, G. D. *J. Phys. Chem.* **1987**, *91*, 1073–1079.

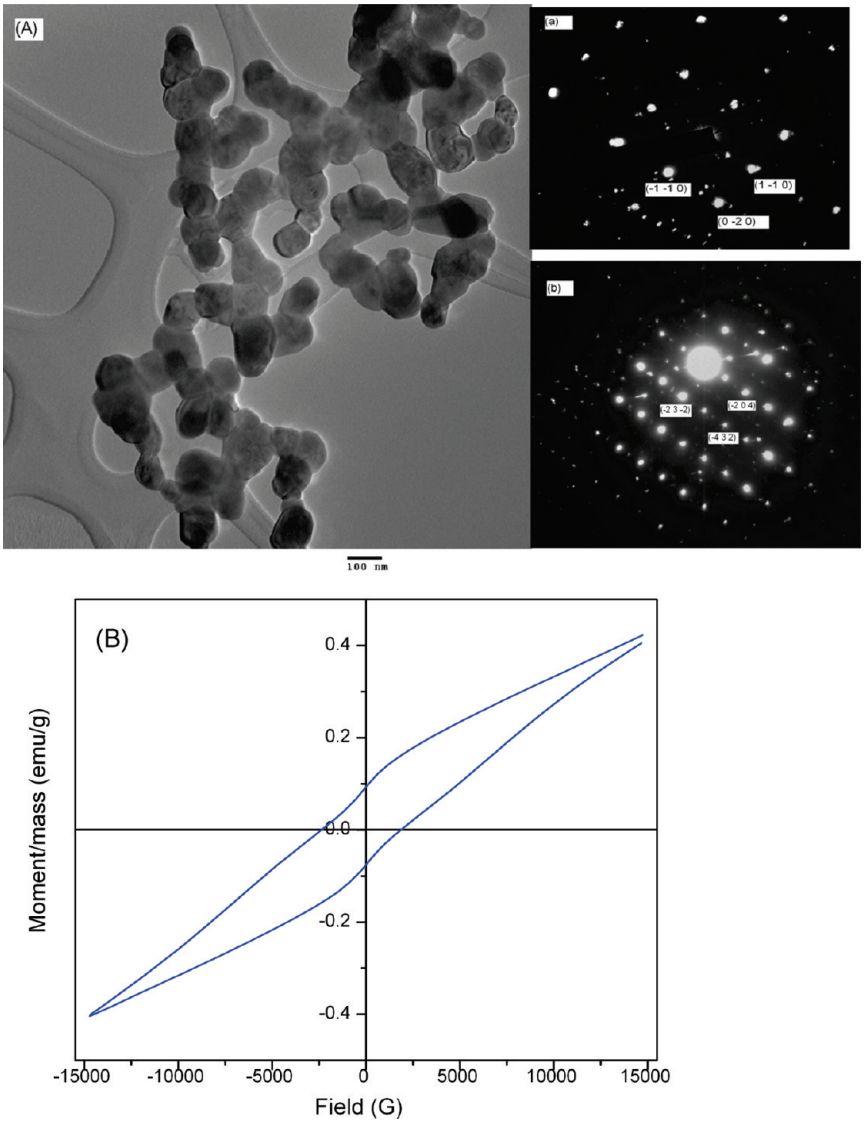

Figure 5. (A) Bright field TEM michrograph of Nd−Fe−B oxide prepared by the sol−gel method. The SADP patterns are indexed to (a) Nd_2O_3 and (b) Fe_2O_3 phases. (B) Room temperature VSM of Nd−Fe−B oxide.

perhaps because the mass fraction of B_2O_3 phase formed at 600 and 700 °C was below the XRD detection limit. In summary, annealing of Nd−Fe−B gel at 800 °C resulted in the formation of Fe_2O_3, $NdFeO_3$, Nd_2O_3, and B_2O_3 phases. The Nd−Fe−B oxide was further characterized by TEM and VSM. The synthesized Nd−Fe−B oxide was found to be 100 nm sized randomly distributed Fe_2O_3, $NdFeO_3$, Nd_2O_3, and B_2O_3 phases (Figure 5A). The room temperature VSM result showed that the Nd−Fe−B oxide had a coercivity of 2.8 kOe and a saturation magnetization of 0.4 emu/g (Figure 5B). This oxide mixture was used in the reduction−diffusion process, as described below to form the desired $Nd_2Fe_{14}B$ phase.

3.1.3. $Nd_2Fe_{14}B$ Phase Formation by Reduction−Diffusion. For the reduction−diffusion process, the oxide powder was mixed with CaH_2 in a nitrogen glovebox and compressed to form a green compact. The compact pellet was then annealed at 800 °C for 2 h in vacuum. Reduction−diffusion of Nd−Fe−B gel annealed at temperatures below

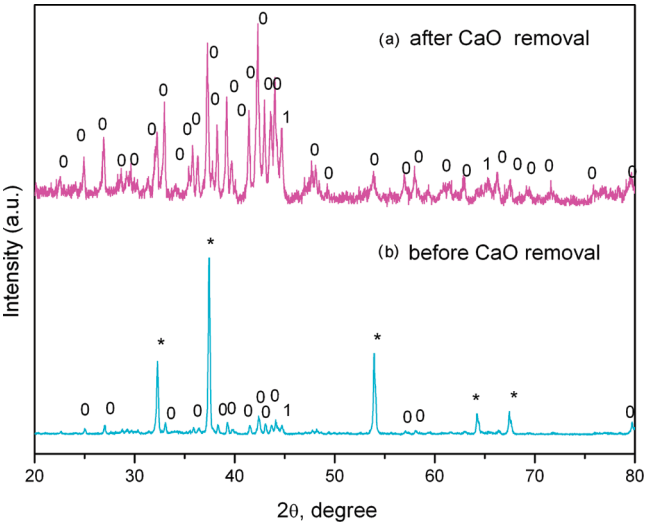

Figure 6. XRD pattern of $Nd_2Fe_{14}B$ prepared by sol−gel followed by the reduction diffusion process (a) before CaO removal and (b) after CaO removal; 1, α-Fe; 0, $Nd_2Fe_{14}B$; ∗, CaO.

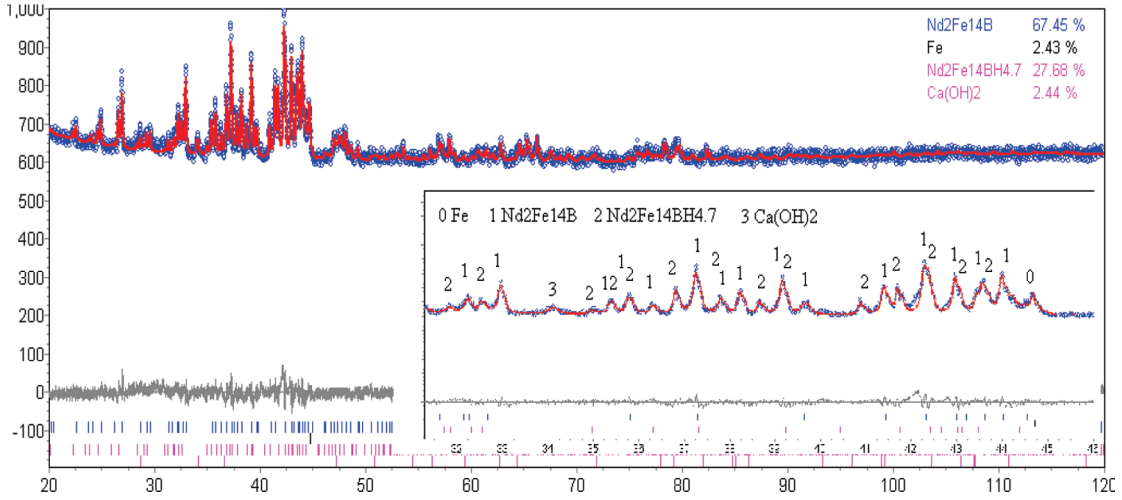

Figure 7. Rietveld analysis of $Nd_2Fe_{14}B$ prepared by sol−gel followed by reduction diffusion. Inset figure shows that peaks corresponding to $Nd_2Fe_{14}BH_{4.7}$ phase are shifted to a lower 2θ of ~0.48, corresponding to 2θ position of $Nd_2Fe_{14}B$ phase.

800 °C did not result in good magnetic properties due to preferential α-Fe phase formation. The resulting reaction product was a mixture of the desired $Nd_2Fe_{14}B$ phase, α-Fe, and byproduct CaO (Figure 6). To remove CaO, the powder was washed with dilute acetic acid and deionized water. CaO was leached out as $Ca(OH)_2$ as a reaction product of H_2O and CaO (eq 1).[29]

$$CaO + H_2O \rightarrow Ca(OH)_2 \qquad (1)$$

The resultant product, determined by Rietveld refinement, was a mixture of three magnetic phases: 67.45 wt % of $Nd_2Fe_{14}B$ (c = 1.2195 nm, a = 0.8797 nm), 27.68 wt % of $Nd_2Fe_{14}BH_{4.7}$ (c = 1.2323 nm, a = 0.89125 nm), and ~2.43% α-Fe (a = 0.2865 nm) and ~2 wt % of $Ca(OH)_2$ (Figure 7). For $Nd_2Fe_{14}BH_{4.7}$ all characteristic peaks were found to be shifted to a lower 2θ values due to unit cell volume expansion of $Nd_2Fe_{14}B$ phase (Figure 7, inset). The crystal size estimated by Rietveld analysis was around 65 nm.

3.2. $Nd_2Fe_{14}B$ Formation Mechanism. *3.2.1. Differential Scanning Calorimetry and X-ray Diffraction Analysis.* The isochronal DSC measurements of the mixture of Nd−Fe−B oxide and CaH_2 powder (Figure 8A) showed that the reduction−diffusion process occurred in three steps: at temperatures of 300, 620, and 692 °C. At these three peak temperatures, the reaction mixture was heated for 2 h in vacuum and analyzed by XRD (Figure 8B,C). The XRD analysis showed that reduction of Fe_2O_3 took place at 300 °C, resulting in the formation of the α-Fe phase. At 620 °C, Nd_2O_3 and $NdFeO_3$ were reduced to form the NdH_2 and α-Fe phases. At 692 °C, the desired $Nd_2Fe_{14}B$ phase was formed.

3.2.2. Thermodynamic Calculations and Reaction Mechanism. To estimate the free energy changes involved, thermodynamic data for the oxides were obtained from Barin.[37] The free energy of formation of $NdFeO_3$ was calculated from

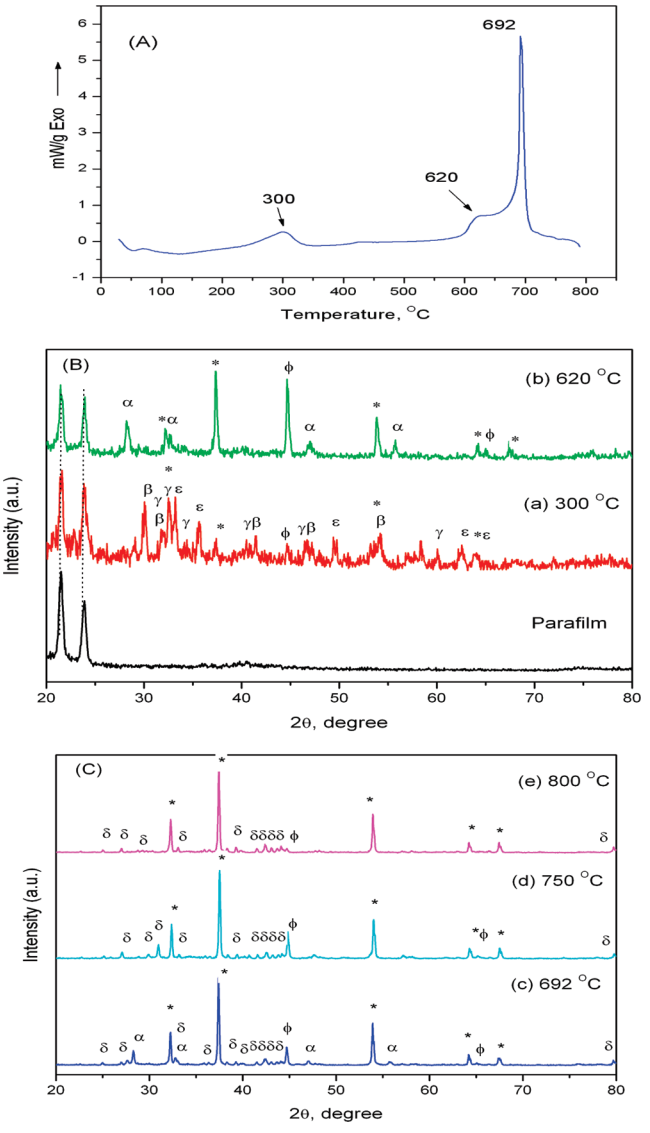

Figure 8. (A) Isochronal DSC of Nd−Fe−B oxide + CaH_2; (B, C) XRD pattern of Nd−Fe−B oxide + CaH_2 heated at temperatures (a) 300 °C, (b) 620 °C, (c) 692 °C, (d) 750 °C, and (e) 800 °C for 2 h in vacuum; ∗, CaO; ϕ, Fe; ε, Fe_2O_3; δ, $Nd_2Fe_{14}B$; γ, $NdFeO_3$; β, CaH_2; α, NdH_2.

(37) Barin, I. *Thermodynamical data of pure substances*; VCH Publications: New York, 1989.

Table 1. Free Energy Changes ΔG for the Reduction Reactions

reaction no.	reaction	ΔG (kJ mol^{-1}) at 600 K (~300 °C)	ΔG (kJ mol^{-1}) at 900 K (~620 °C)
1	$Nd_2O_3 + 3CaH_2 \leftrightarrow 2Nd + 3CaO + 3H_2$	210.6	94.5
2	$Nd_2O_3 + 3CaH_2 \leftrightarrow 2NdH_2 + 3CaO + 2H_2$	1.2	−21.9
3	$NdFeO_3 + 3CaH_2 \leftrightarrow Nd + Fe + 3CaO + 3H_2$	−231.1	−349.3
4	$NdFeO_3 + 3CaH_2 \leftrightarrow NdH_2 + Fe + 3CaO + 2H_2$	−335.9	−407.5
5	$Fe_2O_3 + 3CaH_2 \leftrightarrow 2Fe + 3CaO + 3H_2$	−762.9	−872.485
6	$B_2O_3 + 3CaH_2 \leftrightarrow 2B + 3CaO + 3H_2$	−311.7	−417.2
7	$B_2O_3 + 3CaH_2 \leftrightarrow B_2H_6 + 3CaO$	−167.8	−210.8
8	$B_2O_3 + 3CaH_2 \leftrightarrow 2BH + 3CaO + 2H_2$	466.8	302.1

$\Delta H°$ and $\Delta S°$ of formation values;[38] $\Delta H°$ and $\Delta S°$ were assumed to be constant with temperature. For free energy change of reduction (ΔG) calculations, a mechanism similar to that suggested by Meerson et al.[39] was considered. The reduction of the Nd−Fe−B oxides (M_nO_m, M = Nd, Fe, B) by CaH_2 involved the following reactions (eqs 2−5):

$$CaH_2 \leftrightarrow Ca + 2H \tag{2}$$

$$M_nO_m + mCa \leftrightarrow nM + mCaO \tag{3}$$

$$M + xH \leftrightarrow MH_x \tag{4}$$

$$2H \leftrightarrow H_2\uparrow \tag{5}$$

For the above reactions, thermodynamic (ΔG) calculations for the reduction of these oxides were calculated (Table 1). The free energy change of reduction of Nd_2O_3 at 600 K (~300 °C) is positive (+210 kJ mol^{-1} and +1.7 kJ mol^{-1}), suggesting that the reduction of Nd_2O_3 was thermodynamically not feasible at this temperature. For Fe_2O_3 and B_2O_3, the free energy change at 600 K (~300 °C) is negative (−762.97 kJ mol^{-1}, −311.676 kJ mol^{-1}), implying that the reduction can take place at 300 °C. This was substantiated by the XRD results which showed α-Fe formation. The XRD analysis also showed that the reaction product of Nd−Fe−B oxide and CaH_2 mixture heated at 300 °C still had some unreduced Fe_2O_3 (Figure 8B), perhaps due to kinetic reasons. The free energy of formation of boron and boron hydride showed that the formation of elemental boron, rather than boron hydride as a reduction product is thermodynamically more favorable. This confirmed the minimal loss of boron as volatile boron hydride. Boron crystallizes above 1800 °C,[40] since the synthesis temperature was much lower than this crystallization temperature, the boron was amorphous and not detected by XRD. Although the free energy change values suggest that $NdFeO_3$ reduction was thermodynamically feasible at 300 °C, Nd or NdH_2 were not detected by XRD for this heat treatment condition. $NdFeO_3$ was reduced at 620 °C to NdH_2 and α-Fe; this is a thermodynamically more favorable reaction (Table 1). From both XRD observations (Figure 8B) and the calculated free energy change of reaction for Nd_2O_3 reduction (Table 1), it was concluded that reduction of Nd_2O_3 to form NdH_2 took place at 620 °C. The desired $Nd_2Fe_{14}B$ phase was formed at 692 °C. With increasing temperature and time, the mass fraction of the $Nd_2Fe_{14}B$ phase increased at the expense of NdH_2 and α-Fe phases. On the basis of these observations, the following reaction mechanisms are proposed (eqs 6−10):

$$\text{Step 1 at 300°C}: \quad Fe_2O_3 + 3CaH_2 \rightarrow 2Fe + 3CaO + 3H2\uparrow \tag{6}$$

$$B_2O_3 + 3CaH_2 \rightarrow 2B + 3CaO + 3H_2\uparrow \tag{7}$$

$$\text{Step 2 at 620°C}: \quad Nd_2O_3 + 3CaH_2 \rightarrow 2NdH_2 + 3CaO + H_2\uparrow \tag{8}$$

$$NdFeO_3 + 3CaH_2 \rightarrow NdH_2 + Fe + 3CaO + 2H_2\uparrow \tag{9}$$

$$\text{Step 3 at 692°C}: \quad 2NdH_2 + 14Fe + B \rightarrow Nd_2Fe_{14}B + 2H_2\uparrow \tag{10}$$

Temperatures of 800 °C were needed for the completion of the reduction−diffusion process in a short period of time. The unoxidized Ca metal reacted with H_2O during washing. This led to the liberation of hydrogen (eq 11). The liberated hydrogen was adsorbed into $Nd_2Fe_{14}B$, resulting in some hydride formation (eq 12):[41]

$$Ca + 2H_2O \rightarrow Ca(OH)_2 + H_2\uparrow \tag{11}$$

$$Nd_2Fe_{14}B + xH_2 \rightarrow Nd_2Fe_{14}BH_{2x} \tag{12}$$

3.3. Microstructure and Magnetic Properties. The room temperature VSM results showed that the as-synthesized powder had a coercivity of 6.1 kOe and a saturation magnetization of 20.7 emu/g, resulting in a $(BH)_{max}$ of 0.4 MGOe (Figure 9A). The saturation magnetization was low due the to the presence of nonmagnetic CaO. After removal of CaO by washing, the saturation magnetization increased to 102.3 emu/g but the coercivity decreased to 3.9 kOe, resulting in a BH_{max} of 2.5 MGOe. A magnetic dead layer or chemical inhomogeneity can cause reduction of coercivity.[42,43] However, such phases were not detected by XRD analysis. The coercivity

(38) Parida, S. C.; Dash, S.; Singh, Z.; Prasad, R.; Jacob, K. T.; Venugopal, V. *J. Solid. State. Chem* **2002**, *164*, 34–41.
(39) Meerson, G. A.; Kolchin, O. P. *At. Energ.* **1957**, *2*, 305–312.
(40) Boulanger, J. L.; Autissier, D. *J. Phys.* **1993**, *3*, 1305.
(41) Ram, S.; Joubert, J. C. *Appl. Phys. Lett.* **1992**, *61*, 613–615.
(42) Brunsman, E. M.; Scott, J. H.; Majetich, S. A.; McHenry, M. E.; Huang, M. Q. *J. Appl. Phys.* **1996**, *79*, 5293–5295.
(43) Kirkpatrick, E. M.; Majetich, S. A.; McHenry, M. E. *IEEE Trans. Magn.* **1996**, *32*, 4502–4504.

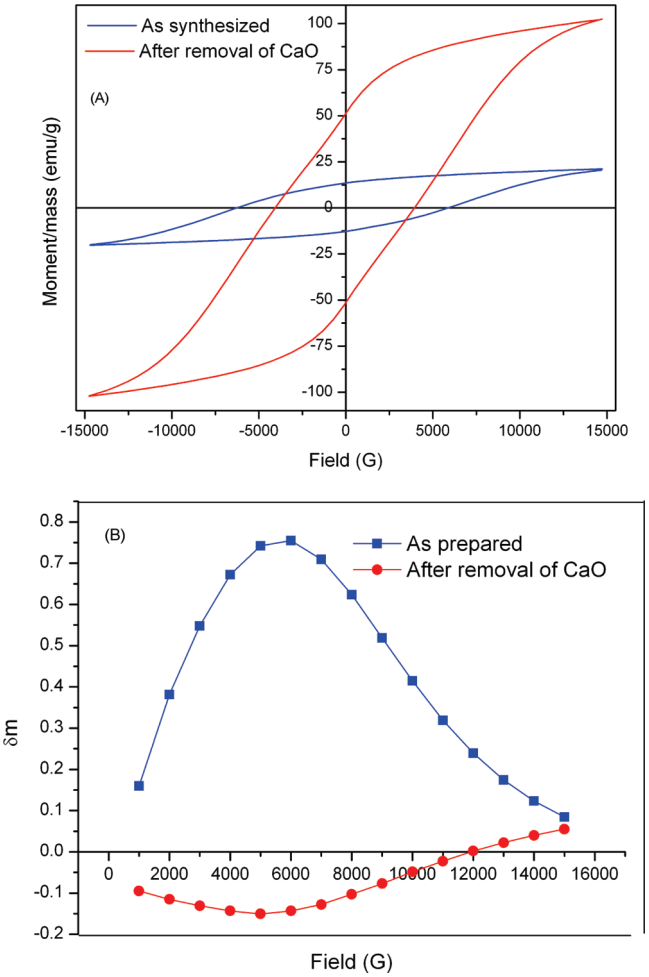

Figure 9. (A) Room temperature VSM of $Nd_2Fe_{14}B$ synthesized by sol−gel followed by the reduction−diffusion method. (B) Henkel plots of $Nd_2Fe_{14}B$ synthesized by sol−gel followed by the reduction−diffusion method.

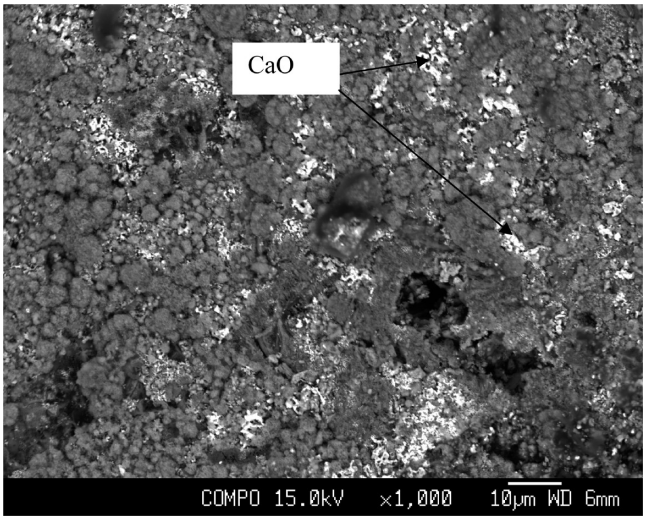

Figure 10. Back scattered electron micrograph of as-synthesized powder. The white patches are the CaO phase.

decrease may be due to the formation of low coercivity $Nd_2Fe_{14}BH_{4.7}$ phase during washing.[44] Interparticle interactions can also affect the coercive field and the reversal mechanism.[45] The interactions between the magnetic

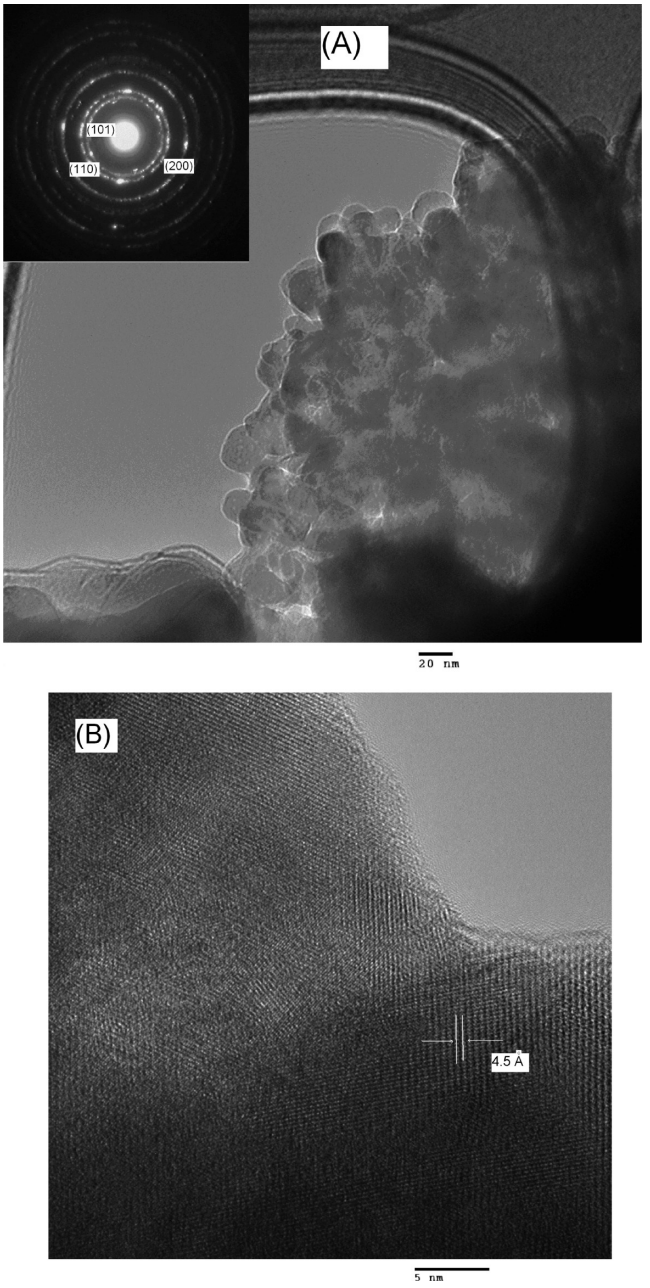

Figure 11. (A) Brightfield TEM micrograph of $Nd_2Fe_{14}B$ synthesized by sol−gel followed by the reduction−diffusion method. The SADP is indexed to the $Nd_2Fe_{14}B$ phase. (B) HRTEM image of nanocrystalline $Nd_2Fe_{14}B$. The interplanar spacing is measured to be 4.5 Å and is closed to the interplanar distance of 4.4 Å between the (200) plane of tetragonal $Nd_2Fe_{14}B$.

grains can be quantitatively analyzed by the Henkel plot.[46−48] DC demagnetization $M_d(H)$ and isothermal remanent magnetization $M_r(H)$ were measured and δM

(44) Ram, S.; Claude, E.; Joubert, J. C. *IEEE Trans. Magn.* **1995**, *31*, 2200–2208.
(45) Schrefl, T.; Schmidts, H. F.; Fidler, J.; Kronmuller, H. *J. Magn. Magn. Mater.* **1993**, *124*, 251–261.
(46) Kelly, P. E.; O'Grady, K.; Mayo, P. I.; Chantrell, R. W. *IEEE Trans. Magn.* **1989**, *25*, 3881–3883.
(47) Bissell, P. R.; Chantrell, R. W.; Lutke-Stetzkamp, H. J.; Methfessel, S.; Spratt, G. W. D.; Wohlfarth, E. P. *J. Phys. Colloq.* **1988**, *12*, C8-1925–C8-1926.
(48) Gao, R.; Chen, W.; Zhang, J.; Fong, W.; Li, W.; Li, X. *J. Mater. Sci. Technol.* **2001**, *17*, 93–96.

was calculated using the following relationship (eq 13).

$$\delta M = [M_d(H)/M_r(\infty)] - [1 - 2 \times \{M_r(H)/M_r(\infty)\}] \quad (13)$$

Here, $M_r(\infty)$ is the remanence after saturation magnetization. The δM plot is called the Henkel plot; for noninteracting single domain particles, δM is zero.[48] If δm is positive, the intergrain interaction is exchange coupling; negative δM suggests that magnetostatic interaction is dominant.[48−52]

Interestingly, the as-synthesized powder showed a positive δM (Figure 9B); i.e., the magnetic phases were exchanged coupled, implying that the magnetic phases were either not completely separated or separation was less than the exchange length (L_{ex}).[50] The back scattered electron micrograph (Figure 10) showed that the nonmagnetic CaO phase was in isolated patches. The magnetic $Nd_2Fe_{14}B$ grains were in close contact and were, therefore, exchange coupled. On the other hand, the δM of the washed powder was negative, suggesting that dipole−dipole interaction was dominant. The bright field TEM micrograph of washed powder (Figure 11A) showed that the particles were agglomerated and ∼50 nm in size; the selected area diffraction pattern (SADP) was indexed to the $Nd_2Fe_{14}B$ phase. Figure 11B showed the HRTEM image of $Nd_2Fe_{14}B$ magnets with an interfringe spacing of ∼4.5 Å. This spacing is closed to interplanar distance of (200) planes in tetragonal $Nd_2Fe_{14}B$. The presence of both dipolar and exchange interactions in the washed samples indicated the presence of grain boundary anisotropy.[53] The anisotropy developed due to the hydrogenation induced amorphization at $Nd_2Fe_{14}B$ grain boundaries during washing can lead to dipolar interactions.[54] Increasing dipolar interactions decreases coercivity and remanence.[55,56] Hence, the washed powder, in which dipolar interactions are predominant, exhibited a low remanent magnetization and energy product (∼2.5 MGOe).

4. Conclusions

Sol−gel followed by reduction diffusion was used to synthesize $Nd_2Fe_{14}B$ magnetic nanoparticles. The mechanism of formation of these nanoparticles was studied. Magnetic properties, phase analysis, and microstructural investigations were performed by FTIR, NMR, VSM, XRD, FESEM, and TEM techniques. (1) Nd−Fe−B gel was prepared from the corresponding salts of Nd, Fe, and B using citric acid and ethylene glycol as gelating agent. The FTIR and NMR results showed that the gel was a Nd−Fe−B citrate complex cross-linked by ethylene glycol. (2) Annealing of the gel at 800 °C resulted in the formation of the Nd_2O_3, $NdFeO_3$, Fe_2O_3, and B_2O_3. (3) Reduction−diffusion was a three step process: At 300 °C, Fe_2O_3 and B_2O_3 reduced to α-Fe and B. At 620 °C, the reduction of Nd_2O_3 and $NdFeO_3$ took place to form NdH_2 and α-Fe. The $Nd_2Fe_{14}B$ phase formed from NdH_2, Fe, and B at 692 °C. (4) The as-synthesized powder was a mixture of the desired $Nd_2Fe_{14}B$ phase, α-Fe, and byproduct CaO. After removal of CaO by washing, the resultant product was a mixture of $Nd_2Fe_{14}B$, $Nd_2Fe_{14}BH_{4.7}$, and α-Fe phases. (5) The magnetic interactions were calculated by the Henkel plot; the as-synthesized powder was exchange coupled whereas the removal of CaO led to dipolar interactions.

Acknowledgment. The authors are grateful to the SERC, Singapore for financial support for this work through ASTAR Grant No. 062 101 0032. The authors would like to acknowledge Prof. Victorino Franco for his important technical suggestions and helpful discussion.

(49) Wohlfarth, E. P. *J. Appl. Phys.* **1958**, *29*, 595–596.
(50) Liu, Z. W.; Davies, H. A. *J. Phys. D: Appl. Phys.* **2009**, *42*, 145006.
(51) Che, X.-D.; Bertram, H. N. *J. Magn. Magn. Mater.* **1992**, *116*, 121–127.
(52) Chen, Q.; Ma, B. M.; Lu, B.; Huang, M. Q.; Laughlin, D. E. *J. Appl. Phys.* **1999**, *85*, 5917–5919.
(53) Joseyphus, R. J.; Narayanasamy, A.; Prabhu, D.; Varga, L. K.; Jeyadevan, B.; Chinnasamy, C. N.; Tohji, K.; Ponpandian, N. *Phys. Status Solidi C.* **2004**, *1*, 3489–3494.
(54) Ram, S. *Phys. Rev. B* **1994**, *49*, 9632–9638.
(55) Du, H. F.; Du, A. *Phys. Status Solidi B* **2007**, *244*, 1401–1408.
(56) Kechrakos, D.; Trohidou, K. N. *J. Magn. Magn. Mater.* **2003**, *262*, 107–110.